JOURNAL OF GEOPHYSICAL RESEARCH, VOL. 100, NO. B1, PAGES 543–559, JANUARY 10, 1995

Geologic investigations of a "slip gap" in the surficial ruptures of the 1992 Landers earthquake, southern California

James A. Spotila and Kerry Sieh
Division of Geological and Planetary Sciences, California Institute of Technology, Pasadena

Abstract. A 3-km-long gap in the dextral surficial rupture of the 1992 M_W = 7.3 Landers earthquake occurs at the north end of a major fault stepover between the Johnson Valley and Homestead Valley faults. This gap is situated along a segment of the Landers rupture that has been modeled geophysically as having a deficit in average slip at depth. To better evaluate the nature of the slip gap, we document in detail the character and distribution of surficial rupture within it. Along the gap, is a northwest trending thrust fault rupture with an average of less than 1 m of northeast directed reverse-slip and nearly no oblique right slip. We interpret this rupture to be limited to the shallow crust of the northern end of the stepover and to have been the secondary result of dextral shear, rather than a mechanism of rigid-block slip-transfer from the Landers-Kickapoo fault. A zone of en echelon extensional ruptures also occurs along the slip gap, which we interpret as the secondary result of diffuse dextral shear that accommodated less than 0.5 m of west-northwest extension. These secondary ruptures represent a discontinuity in the surficial dextral rupture of the Landers earthquake, which we propose resulted from the lack of a mature fault connection between the Johnson Valley and Homestead Valley faults. The rupture pattern of the slip gap implies a significant deficit in net surficial slip, which compares favorably with some geophysical models. Aspects of this rupture pattern also suggest a temporal sequence of rupture that compares favorably with geophysical interpretations of the dynamic rupture propagation.

Introduction

Coseismic fault ruptures commonly consist of solitary principal fault segments, but in some cases, rupture in a single earthquake propagates beyond one discrete fault segment to another. This was the case with the M_W = 7.3 Landers earthquake of June 28, 1992, during which dextral shear was distributed on six major fault segments separated by complex 1- to 3-km-wide fault stepovers (Figure 1) [*Sieh et al.*, 1993]. One of these complex stepovers is a dilational jog 17 km north of the mainshock epicenter, between the dextral Johnson Valley and Homestead Valley faults (JVF and HVF) (Figure 2) [*Sieh et al.*, 1993]. The northern end of this stepover is a region of complex surficial faulting characterized by a lack of dextral slip; we term this region the Homestead Valley (HV) slip gap. The fresh surficial ruptures in this slip gap offered an unusual opportunity to investigate the interactions and evolution of active faults in a structural stepover.

The HV slip gap is located along a section of the Landers rupture that experienced an apparent deficit in average slip relative to two distinct high-slip sections of rupture to the north and south, which was identified by early seismologic investigations [*Kanamori et al.*, 1992; *Sieh et al.*, 1993; *Campillo and Archuleta*, 1993]. Owing to their limited resolution and nonuniqueness, these geophysical studies cannot resolve whether this deficit reflects a discontinuity in the rupture at depth. Such a discontinuity would indicate that the Landers earthquake was a double event, caused by two spatially and temporally distinct ruptures. More recent studies, however, present complex, nonunique dislocation models based on seismic and geodetic data, which suggest that the rupture in the HV slip gap was continuous at depth and characterized by reduced slip and a delay in dynamic propagation [*Wald and Heaton*, 1994; *Cohee and Beroza*, 1994]. Resolving aspects of the rupture pattern that are ambiguous in these geophysical models, such as whether the rupture was discontinuous and, if so, what prevented continuous rupture and how slip was transferred across the discontinuity, is important to the study of interacting active faults.

This paper is a detailed geologic investigation of the surficial ruptures within the HV slip gap. Unlike remotely sensed seismic and geodetic data, which must be inverted to model slip distribution and rupture dynamics and have limited resolution, surficial displacements and rupture geometries are directly observable expressions of the kinematics and dynamics of the rupture. These geological data are therefore a unique and critical source of information for interpreting the Landers rupture pattern. In combination with the detailed and abundant seismic and geodetic data, the well-exposed surficial ruptures provide an unprecedented opportunity to study coseismic rupture processes and the long-term tectonic evolution of an active fault stepover.

Field Methods

In the week immediately following the Landers mainshock, we were part of a team of geologists that mapped the surficial ruptures and collected hundreds of measurements of vertical and lateral fault offsets along the entire rupture zone

Copyright 1995 by the American Geophysical Union.

Paper number 94JB02471.
0148-0227/95/94JB-02471$05.00

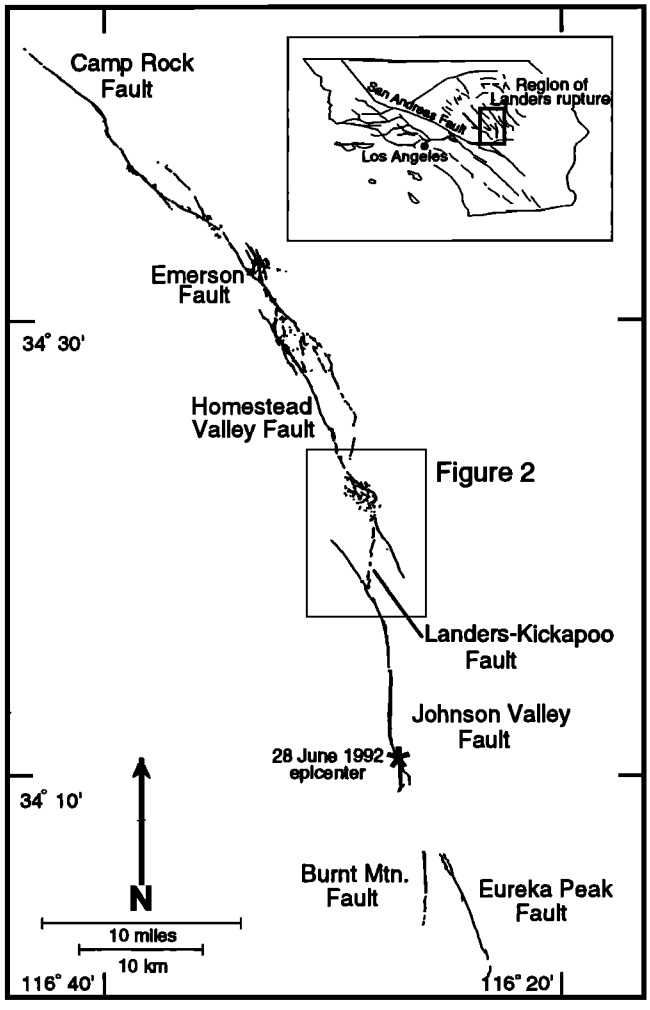

Figure 1. Map of the Landers earthquake surficial rupture in southern California [from *Sieh et al.*, 1993]. In this paper we discuss the ruptures in the stepover between the Johnson Valley and Homestead Valley faults. The June 28, 1992, mainshock epicenter is shown along the Johnson Valley fault with a star.

[*Sieh et al.*, 1993]. In July and August 1992, J. A. Spotila mapped the surficial faulting in the HV slip gap in greater detail and measured many more offsets. In order to determine whether any throughgoing surficial faulting was present along the HV slip gap, we made numerous transects perpendicular to the trend of the fault zone. Fractures with more than 1 cm of lateral or vertical offset were mapped at a scale of 1:6000 on topographic maps or aerial photographs. We traced all fractures with vertical or strike-slip offset along their entire length or to their connections with the throughgoing dextral ruptures at the ends of the slip gap. Less prominent fractures were mapped only along transects but, due to their ubiquity, not necessarily to their full extent.

We determined the along-strike component of horizontal displacement on fractures by matching crack edges or linear features such as tire tracks, channels, and road edges across the fractures. The total lateral offset across a zone of fractures was determined by summing the offsets of single fractures across the zone. This differed from measurements in the more urban regions of the Landers rupture zone to the south, where far-field determinations of lateral offset were possible due to the presence of straight dirt roads and lines of utility poles. We also measured vertical offsets across all fractures. We interpreted the sense of vertical motion on non–strike-slip fractures to be normal where open fissures were present or a dipping normal fault surface could be identified. We also identified thrust fault ruptures by their characteristic scarps (see observation section, Figures 3a and 3b). Dips of these faults were obtained using the "rule of v's" on the surficial trace and topography and by direct measurement where the fault surface was exposed in channels or hand-dug trenches. We estimated net dip slip for the thrust faults from fracture dip, vertical displacement, ground slope, and dimensions of the collapsed hanging wall (Figure 3c).

The degree and style of fracture exposure and preservation depended on the surficial material. Fractures on hard, flat alluvial surfaces were typically well-exposed and well-preserved, whereas fractures in sand or talus or on steep bedrock or colluvial slopes were commonly difficult to recognize and were less pervasive. Because our field work was completed in the summer months and soon after the rupture, there was no degradation of fractures due to precipitation. However, fractures in loose sand were degraded by wind erosion, and after 2 months many fractures in sand had disappeared.

Observations

The JVF-HVF stepover and the HV slip gap are among the more geometrically complex portions of the 1992 Landers surficial rupture (Figures 1 and 2). Our field mapping confirmed that no throughgoing dextral surficial rupture occurred in 1992 along a 3-km section of the HVF (as mapped by *Dibblee* [1967]) between the northern and southern segments of HVF rupture (NHVF and SHVF, respectively). This dextral slip gap is directly north of the termination of the Landers-Kickapoo fault (LKF) (Landers fault of *Sieh et al.* [1993] and Kickapoo fault of *Hart et al.* [1993]) and SHVF ruptures and is occupied by a hill of quartz monzonite (Figure 2). The NHVF and SHVF become diffuse zones of en echelon fractures in loose sandy alluvium and colluvium as they near the hill and then terminate. The LKF and SHVF come within about 100 m of merging with each other 1 km south of the slip gap, and the SHVF assumes the same northerly trend as the LKF to the north of the LKF's termination (Figure 2). Dextral surficial displacements greater than 2 m on the LKF, SHVF, and NHVF decrease rapidly to zero as they approach the slip gap (Figure 4). Representative lateral and vertical offsets for the major ruptures in the JVF-HVF stepover are shown in Figure 2.

Thrust Fault

Although there are no major strike-slip ruptures within the HV slip gap, there is a 3.1-km-long thrust fault rupture along the northeast flank of the hill between the NHVF and SHVF (Figure 5 and Table 1). Movement on this N52°W, southwest dipping thrust fault formed a distinctive scarp in both loose sandy and hard gravely alluvium (Figure 3a). This scarp is characterized by a disaggregated wedge of the hanging wall block covering a part of the footwall ground surface, which is separated from the intact, undeformed hanging wall block by tensile fractures (Figures 3b and 3c). The thrust fault has interesting geometric relations with the neighboring strike-

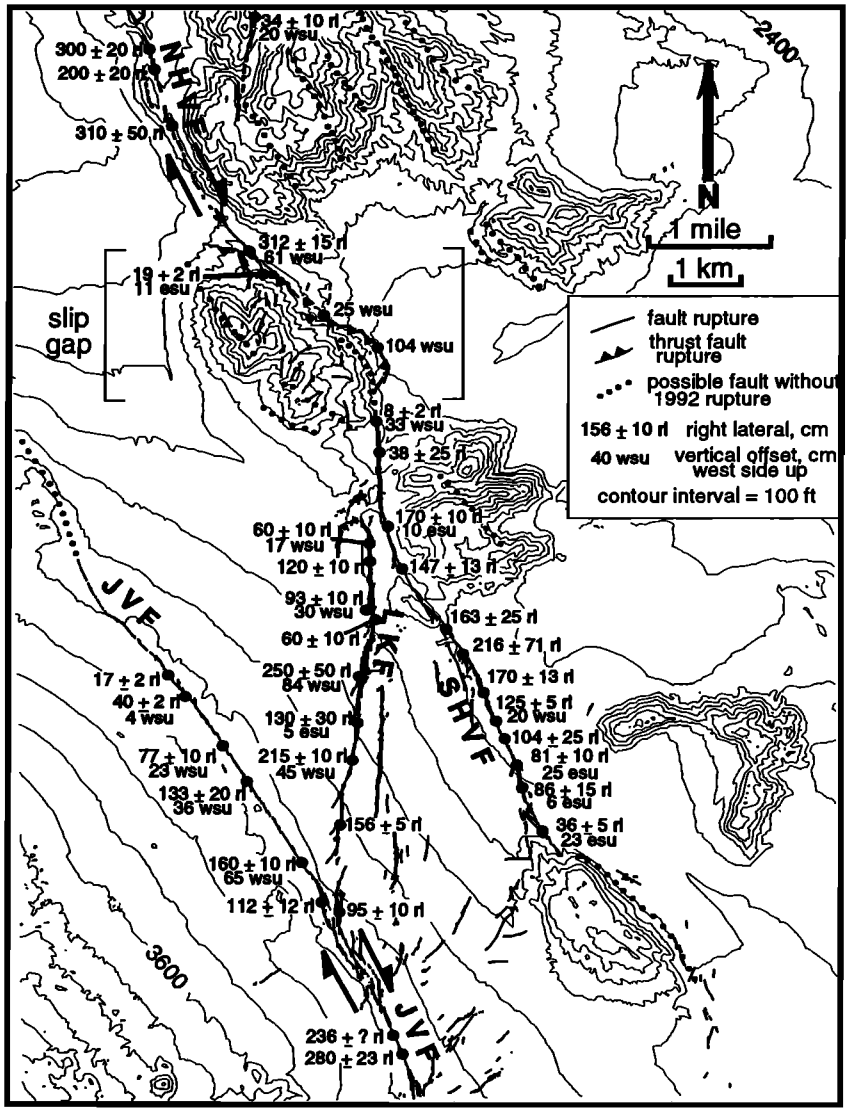

Figure 2. Map of the JVF-HVF stepover and HV slip gap. Surficial ruptures are solid dark lines, topographic contours are thin lines, and possible preexisting faults without 1992 rupture are dotted lines. Representative offset measurements are included for the major ruptures. Some minor 1992 fractures south of the LKF between the JVF and SHVF are from *Bryant* [1992]. NHVF, Northern Homestead Valley fault; LKF, Landers-Kickapoo fault; SHVF, Southern Homestead Valley fault; JVF, Johnson Valley fault.

slip ruptures. Although the thrust is present on both sides of the NHVF and appears to cross it in map view (Figure 5), no thrust scarp is actually present within 25 m of the dextral rupture zone, and therefore neither surficial fault trace offsets the other. At the southern end of the thrust trace, a 100-m-long, northeast trending tear fault that consists of a wide zone of en echelon fractures terminates about 150 m away from the SHVF.

The arcuate trace of the thrust fault wraps around a northeast sloping hillside, primarily at the boundary between the higher, steeply sloping bedrock or colluvium and the gentler sloping alluvial surfaces below (Figure 5). Along most of its trace, the thrust cuts thin alluvium or colluvium that is typically less than 10 m thick (based on projection of the hill's bedrock slope under the alluvium). The sinuous, irregular surficial trace is typical of shallow to moderately dipping dip-slip fault ruptures and consists of numerous splays of parallel thrust segments that are commonly discontinuous or connected by tear faults, and which have geometries that are dependent on local topography. The general conformity of the surficial trace to local topography indicates that the fault dips shallowly to the southwest. Along its northern segment, the thrust trace diverges from the hillside and continues across a gently sloping, sandy alluvial surface. At several localities west of the NHVF, the northeast facing scarp crops out on southwest sloping channel walls and therefore is opposed to the local topographic gradient.

Displacement on most of the thrust-fault trace is pure dip slip, with the southwest-side-up and a northeast directed horizontal component of shortening. It was commonly difficult to determine whether there was a strike-slip component to the thrust motion, because linear features that crossed the

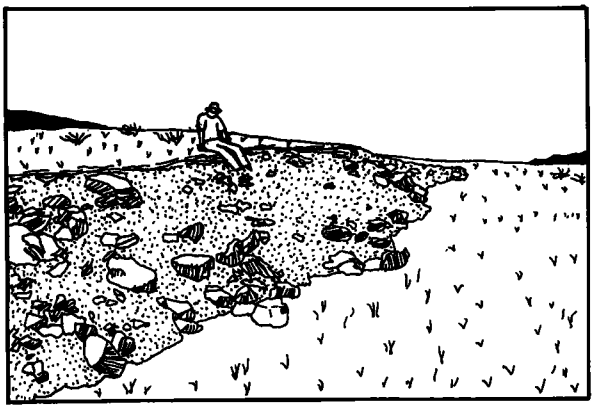

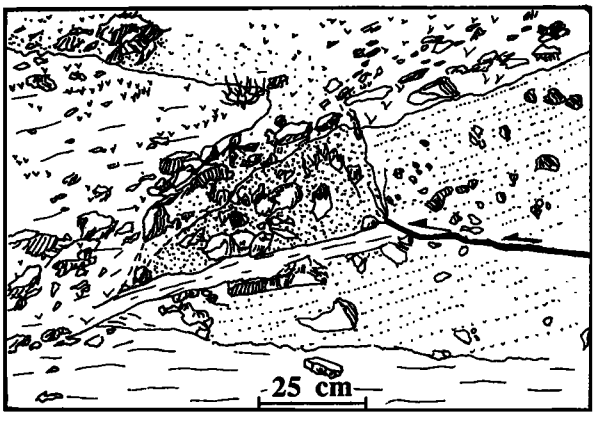

A

B

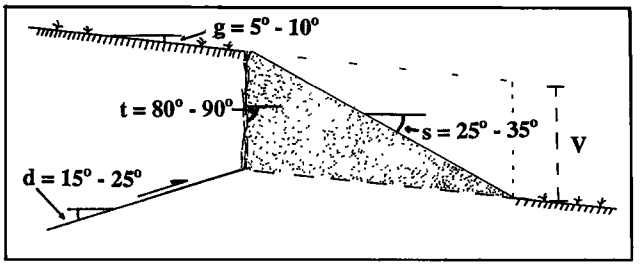

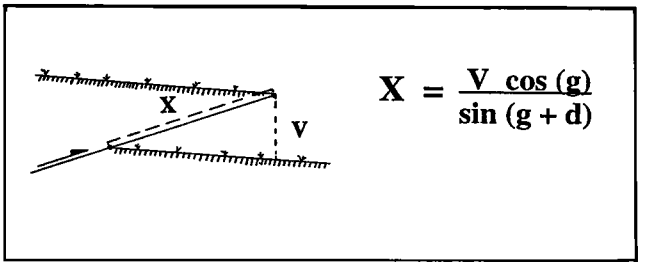

C

Figure 3. Determination of dip slip on the thrust fault in the HV slip gap requires understanding of the geometry of the fault and scarp. (a) Photograph and simplified interpretive drawing of a scarp along the thrust fault at location 10 (shown in Figure 5). View is to the northwest, and vertical offset here is southwest-side-up about 1 m. The stippled surface is the collapsed hanging wall block. (b) Photograph and simplified interpretive drawing of a hand-dug exposure of the thrust fault at location 8 (shown in Figure 5). View is to the southeast, and vertical offset here is southwest-side-up about 25 cm (scale bar and 6-cm-wide tape measure for scale). The stippled surface, which is the collapsed hanging wall block, is separated from bedded alluvium by tensile fractures and overlies a prerupture ground surface. The thrust fault surface is defined by crushed pebbles and a zone of relative weakness in the alluvium. (c) Schematic diagram that illustrates our interpretation of the thrust fault scarp. This cross section, drawn perpendicular to the thrust trend, represents the general case in which the thrust fault plane could be defined, its dip (d) measured, and tensile fractures (t) separated the collapsed hanging wall block from the intact hanging wall block. The ground slope (g) and slope of the collapsed hanging wall (s) were measured in the plane of the trench. A standard range in values for these parameters is given. The bottom drawing shows how we assume the collapsed hanging wall block should be restored. From this assumption, the net dip slip (X) was calculated using the given equation with the fault dip (d), ground slope (g), and vertical offset (V).

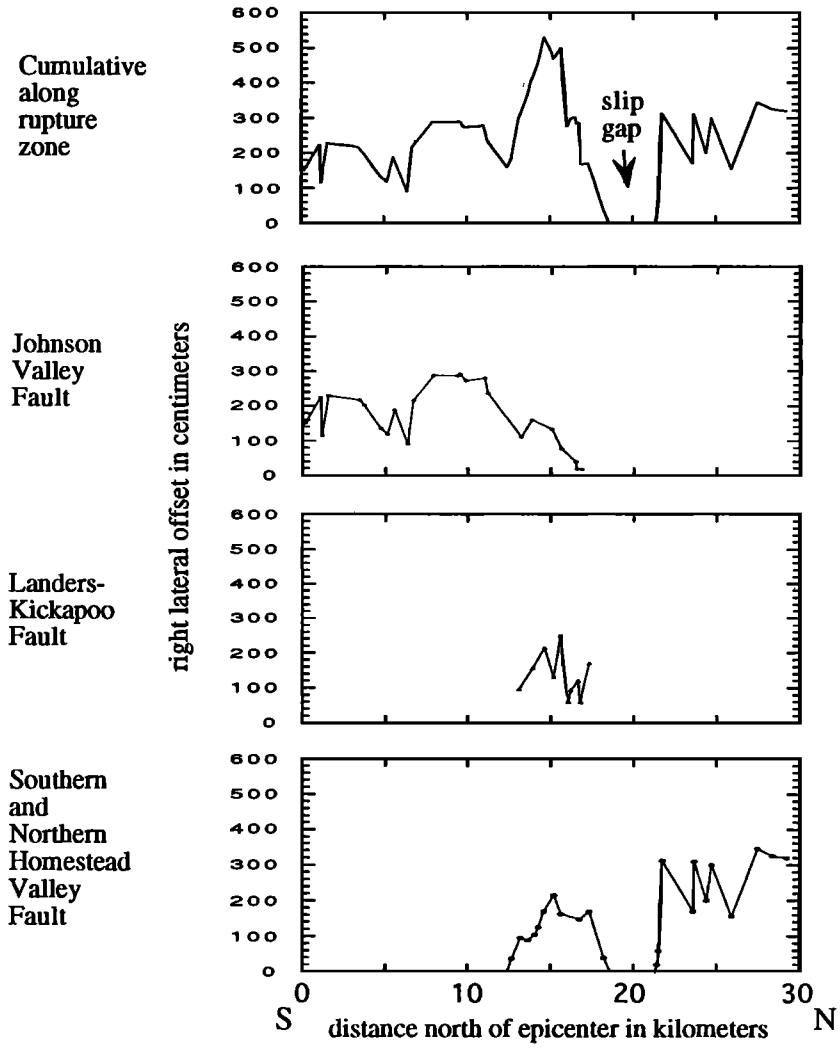

Figure 4. Graph of the distribution of right slip along the JVF, LKF, SHVF, and NHVF, which demonstrates the gap in dextral slip. The top profile shows the cumulative right slip, tabulated by linear interpolation. The location of the HV slip gap is indicated. The displacement along the LKF does not decrease to zero because it joins other ruptures at both ends.

thrust fault obliquely were shortened across it and therefore had apparent lateral displacements. Fortunately, there were many features that were parallel to the gradient of the hill (channel beds, bike tracks) that crossed the thrust fault orthogonally, which we used to determine strike-slip offsets. Of 27 linear features that cross the thrust, 23 showed no strike-slip offset, 18 of which were more or less orthogonal to the thrust scarp (Figure 5 and Table 1b). For the five oblique features, we estimated the amount of apparent lateral offset that should have been present given the obliquity of the feature and the horizontal shortening on the thrust fault (estimated from the estimates of net dip slip on the thrust fault, which are discussed below) and found that in each case it matched the observed lateral displacement to within about 10 cm. Of the four strike-slip offsets we identified (three dextral and one sinistral), two (locations 4 and 5; Figure 5 and Table 1a) occur on segments of the thrust fault that are oblique to the average thrust trend (similar to tear faults), and the other two are much smaller than the net dip-slip or vertical offsets at the same location. All of these strike-slip offsets, as well as the 10-cm uncertainty in our estimates of lateral offsets of oblique features, are significantly smaller than the respective vertical or net dip-slip offsets of the same location. This indicates that the ratio of reverse-slip to strike-slip is very large along the entire thrust trace. We conclude that the motion on the thrust fault was very close to pure reverse and that the minor lateral offsets are localized and probably due to slight changes in the strike of the rupture.

We dug several small trenches across the thrust scarp to investigate its geometry and to determine net dip-slip offsets. In each of these, we identified a southwest dipping fault surface by pulverized bits of rock and centimeter-wide zones of weak disaggregated material within more intact alluvium. This fault surface separates the buried footwall ground surface from the intact hanging wall (Figures 3b and 3c). Direct measurements of the dip of the fault surface agree with the shallow southwest dips determined by the rule of v's. Dip estimates from both methods range from 4° to 29° and average about 20° (Figure 5 and Table 1a). This variation of dips indicates that the thrust fault forms an irregular plane, rather than a smooth curvilinear one. Our hand-dug

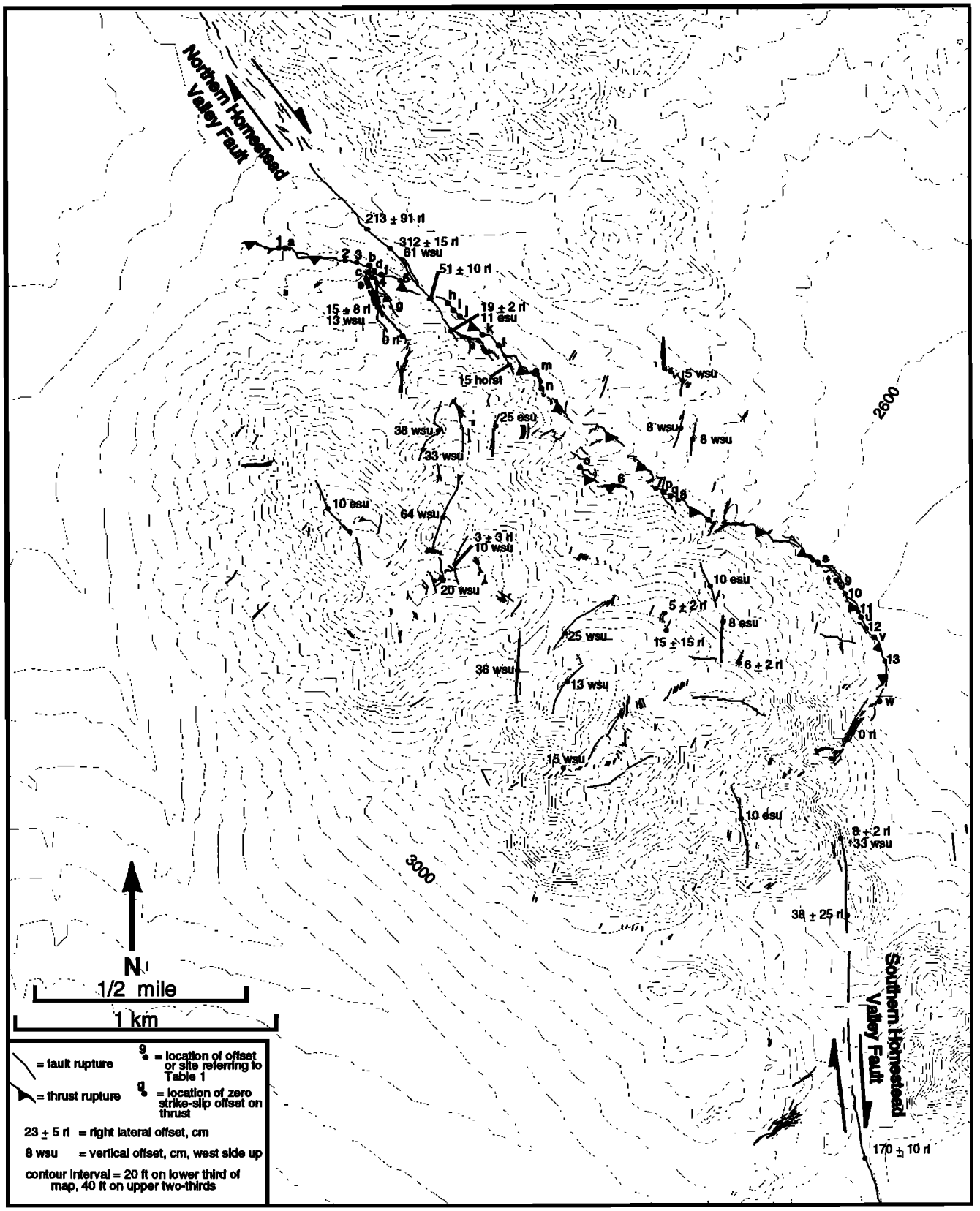

Figure 5. Detailed map of the HV slip gap showing adjacent strike-slip ruptures, the thrust fault rupture, and secondary extensional ruptures. Representative offset measurements are shown, except along the thrust fault. Numbers along the thrust fault refer to 13 sites of detailed measurements shown in Table 1a, and letters along the thrust fault refer to 23 sites of zero strike-slip offset shown in Table 1b.

Table 1a. Measurements of Thrust Fault Offset and Dip

Location	Data Source	Vertical Offset, cm WSU	Strike-Slip Offset, cm	Fault Dip °SW	Dip-Slip Offset, cm
1	trench	74 ± 15	0 (a, Table 1b)	21 ± 5	190 ± 20
2	rule of v's	25 ± 5	?	22 ± 5	...
3	rule of v's	25 ± 5	?	23 ± 5	...
4	shortened bike track	15 ± 5	23 ± 15 RL	22 ± 10	33 ± 10
5	offset track	3 ± 1	10 ± 5 LL	...	...
6	rule of v's	20 ± 5	?	4 ± 3	...
7	channel cut across thrust	...	0 (p, Table 1b)	17 ± 3	...
8	trench	25 ± 8	0 (q, Table 1b)	5 ± 3	89 ± 20
9	rule of v's	...	0 (t, Table 1b)	25 ± 5	...
10	trench	103 ± 10	?	20 ± 5	222 ± 40
11	shortened dirt road	34 ± 3	0 (u, Table 1b)	17 ± 5	114 ± 15
12	trench	50 ± 5	20 ± 20 RL	21 ± 5	120 ± 30
13	offset road	34 ± 5	15 ± 10 RL	24 ± 5	85 ± 30

Locations 1–13 are shown in Figure 5. All dip-slip and net slip data that were collected on the thrust fault are given here, although we measured many more vertical offsets (Figure 6) and strike-slip offsets (or lack of strike slip) (Table 1b) on the thrust fault. Dots indicate no data, a zero indicates that value was measured to be zero, and a question mark indicates the value could not be determined. Net dip-slip offsets were calculated as shown in Figure 3c and by extrapolating from the amount of horizontal shortening on the thrust. RL, right-lateral; LL, left-lateral.

trenches were not deep enough to resolve whether the thrust plane becomes more uniform or changes orientation in the shallow subsurface.

The vertical offset on the thrust reaches a maximum of 119 ± 15 cm in the southeast, and averages about 32 cm along its entire length (the appendix, part 1). Large offsets near the southeast and northwest ends of the rupture result in a slip function with a rough saddle shape (Figure 6). Net dip slip on the thrust was determined from the values of dip, the vertical offsets, and the dimensions and orientations of the scarp measured in trenches (Figure 3c and Table 1a). We estimate the maximum net slip to be 222 ± 40 cm southwest over northeast and estimate the average net dip slip (the appendix, part 1) to be about 74 cm. A component of horizontal shortening accompanies this net dip slip. At one location a cemented sand channel is compressed and shortened normal to the thrust trend with less than 20 cm of vertical offset and no strike-slip offset, leaving a 10-m-wide zone of overlapping sand crusts. At two locations we were able to measure the horizontal shortening on linear features that were each intersected and shortened at two separate places along a curved segment of the thrust fault and combine this shortening with vertical offsets and fault dips to estimate the net dip slip (Table 1a).

Table 1b. Features Crossing the Thrust With Zero Strike-Slip Offset

Feature	Description
a	dirt road (oblique)
b	tire tracks
c	dirt road
d	dirt road
e	dirt road (oblique)
f	dirt road (oblique)
g	dirt road
h	tire tracks
i	tire tracks
j	tire tracks
k	tire tracks
l	tire tracks
m	channel bed
n	dirt road
o	channel incision
p	channel incision
q	channel incision
r	channel bed
s	channel bed
t	cemented channel
u	dirt road (oblique)
v	dirt road
w	dirt road (oblique)

Locations a–w are shown in Figure 5. Eighteen of these features were orthogonal or nearly orthogonal to the thrust scarp, so that apparent lateral offset due to horizontal shortening did not have to be determined. The five oblique features (as indicated) were found to have less than 10 cm of strike-slip offset by estimating the amount of apparent lateral displacement that should have been present given the horizontal shortening (estimated from net dip-slip) at that location.

Zone of en Echelon Extension

In addition to the thrust fault, there are smaller, non–strike-slip ruptures in the HV slip gap. We mapped numerous normal fault ruptures along the hill west of the thrust fault. These discontinuous ruptures are typically hundreds of

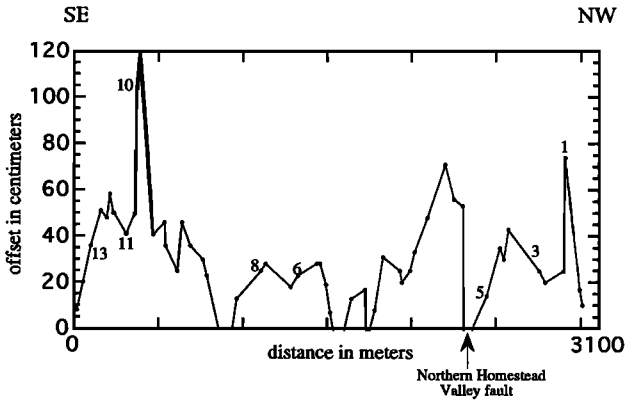

Figure 6. The distribution of southwest-side-up vertical offset along the thrust fault. Numbers refer to locations in Figure 5 and in Table 1a, and the arrow points to the location where the thrust surficial trace is intersected by the NHVF.

meters long and roughly form a broad, left-stepping, weak en echelon pattern along the southward projection of the NHVF (Figure 5). These ruptures consist of either normal fault scarps, open fissures, or grabens with predominantly west-side-up vertical offsets as large as 64 cm (representative offset values are shown in Figure 5). At one location (5 m northwest of location p; Figure 5) a large open fracture cuts obliquely through both the hanging wall and footwall of the thrust fault without being offset across the scarp, which demonstrates that at least one tensile fracture formed after rupture of the thrust fault. We identified small measurable lateral offsets on only four of these ruptures (dextral offsets of 3, 5, 15, and 6 cm) (Figure 5), in marked contrast to the individual en echelon splays along the northern LKF that have over 1 m of right slip (Figure 2). We therefore consider this en echelon fracture zone to be mainly extensional. The average trend of the 33 fractures with >1 cm vertical offset is N09°E (the appendix, part 2), which corresponds to a direction of horizontal extension of N81°W.

Although about half of these fractures have open fissures, the horizontal extension on any particular fracture is not equal to the width of the fissure. This is because the apertures of the fissures appeared to have been widened by collapse of the fissure walls and are discontinuous and occur only along small fractions of the total length of the ruptures. The extension on each fracture must be reflected solely in the vertical offsets along segments of the rupture that have no fissure. These vertical offsets would have a component of horizontal extension if the faults have nonvertical dips. We were not able to measure the dips of these fractures because their exposed surfaces were normally small and poorly preserved, but they generally appeared to be near-vertical. However, it is possible that the dips of these fractures could have been as low as about 75° without appearing nonvertical to the naked eye. To estimate the maximum horizontal extension on each fracture (not including the localized fissures), we used a hypothetical 75° dip, the maximum vertical offsets, and the ground slopes at each fracture. We then summed the net extension distributed across the hill (along the N81°W average extension direction) given the spatial distribution and lengths of these fractures (the appendix, part 3). Our best estimate of the maximum N81°W extension across the hill accommodated by the normal fractures is much less than 0.5 m (the appendix, part 3).

We also identified hundreds of smaller fractures in the HV slip gap that were typically less than 25 m long, had millimeter-sized apertures, and had less than 1 cm of vertical or lateral slip. Some of these fractures occurred in steeply sloping sand or colluvium and appeared to be the result of slumping due to ground shaking, but most others probably resulted from tectonic strain. In most cases, these fractures occurred in discontinuous, narrow bands that were not mapable at 1:6000. Rather than attempting to map all of these in full detail, we noted their orientations and dimensions where we encountered them (Figure 5). These fractures seemed to be distributed roughly evenly across the hill. The density of this distribution was very low, however, and the hill was not nearly as pervasively fractured as the shear zones along the main Landers rupture (such as along the SHVF [*Johnson et al.*, 1994]) (Figure 5). In addition, these fractures were not organized into discrete shear zones that are present elsewhere along the Landers rupture, which are 50–200 m wide, have pervasive extensional and left-lateral fractures, are bounded by narrow fault zones which accommodate most of the zone's dextral displacement, and commonly have mole tracks or other compressional features [*Johnson et al.*, 1994]. We therefore consider these fractures to be minor responses to tensile stress exerted on the hill, rather than a pervasive dextral shear zone. The distribution of these cracks suggests that they did not contribute much extension to that accommodated by the larger normal fractures.

We noted enough of these small tensile fractures to analyze their trends, and define a dominant north-northeast tendency (Figure 7). The correlation coefficient (the appendix, part 4) for fractures within the N05°E to N30°E trend range was 2.4. This implies that the average orientation of these fractures is similar to the N09°E average trend of the larger normal fractures and that both were produced by west-northwest extension.

Slip Distribution Within the HV Slip Gap

The surficial ruptures of the HV slip gap did not accommodate as much slip as the neighboring strike-slip ruptures. The maximum dip slip on the thrust fault resolves to less than 1 m of right slip along the strike of the HVF and the average dip slip resolves to only about 30 cm of right slip, indicating that the thrust fault did not accommodate as much right slip as the LKF/SHVF or NHVF ruptures. Although we could not precisely determine the amount of right slip in the zone of extensional fractures, it does not seem realistic that it could have been more than the 0.5-m maximum extension (but could be less). Thus the average displacements on the thrust fault and the extensional fractures probably accommodate less than a meter of combined right-slip across the slip gap, in contrast to the combined 6 m of right slip to the south (JVF, LKF, and SHVF) and the 3 m of right slip to the north (NHVF) (Figure 2).

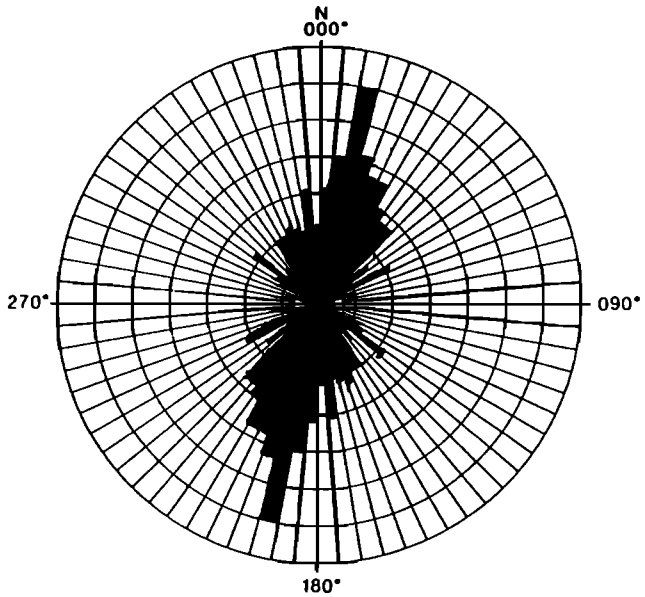

Figure 7. Rose diagram of trends of 322 small extensional fractures in the HV slip gap. Each segment between concentric circles corresponds to five fractures of a given trend. The dominant north-northeast trend of the fractures suggests they may be associated with extension produced by dextral shear along the northwest trend of the NHVF.

Even when net dip slip is added to the strike slip, there appears to be a slip deficit in the gap. Figure 8 shows both the net dip slip along the thrust fault and the extensional fractures in the slip gap (km 19 to 22), as well as the displacement along the adjacent strike-slip ruptures. This figure clearly shows a marked deficiency in net surficial displacement along the 5-km-long reach from km 17 to km 22, even though slip on the secondary ruptures is included. This demonstrates the existence of a surficial slip gap along the Landers rupture.

Interpretations

Our detailed observations of the surficial rupture within the HV slip gap aid in understanding the processes of the 1992 rupture and the tectonic development of the JVF-HVF stepover. In our interpretation of these data, we first consider the likely kinematic relations between various coseismic ruptures and develop a model of the overall rupture pattern in the stepover. This model is developed by showing that a simpler, more intuitive model is inconsistent with our observations. We then discuss geophysical evidence of the slip distribution and the likely dynamic sequence of the 1992 rupture in the HV slip gap. Finally, we discuss the tectonic development of the JVF-HVF stepover and HV slip gap and relate it to the 1992 rupture pattern.

Kinematic Interpretation of the Thrust Fault

Based on their geometric relation, movement on the thrust fault seems to be closely linked to dextral slip on the LKF and on the north trending segment of the SHVF that lies north of the LKF's termination (Figure 2). The north directed motion of the block west of the LKF can easily be envisioned to generate contraction across the thrust fault as a result of rigid block translation, as depicted schematically in Figure 9.

Significant difficulties exist with this simple, rigid block interpretation, however. First, dextral slip on the LKF and SHVF decrease to zero northward, and surficial dextral rupture terminates south of the southeastern end of the thrust fault (Figures 2 and 5). Even though the maximum right slip on the LKF of about 2.5 m is roughly equal to the maximum net dip slip of more than 2 m on the thrust, these offsets are separated by a distance of more than 4 km, along which dextral slip on the LKF decreases to zero and the rupture terminates. This precludes a transformlike junction of the two faults, such as is shown in Figure 9, because such a model predicts that the dextral LKF rupture (or northern SHVF rupture) would directly connect with the thrust.

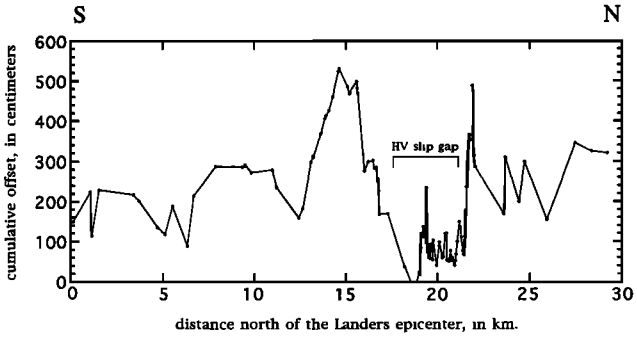

Figure 8. Distribution of cumulative net slip in the JVF-HVF stepover. The right-slip distribution on the major strike-slip faults is taken from Figure 4, and the net dip slip along the thrust and the vertical offset along the en echelon fractures are included. The locations of all offsets were projected onto the N15°W trend of the Landers zone, and the location of the HV slip gap (as shown) was defined by the limits of major surficial strike-slip ruptures (the terminations of the NHVF and SHVF surficial ruptures). Even with the dip slip included, the slip gap remains a 5-km-long trough in the slip distribution.

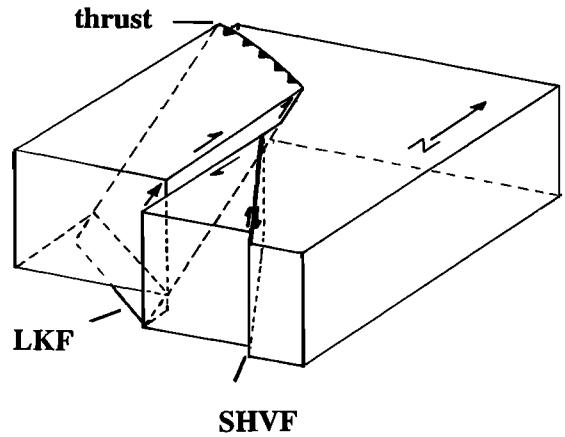

Figure 9. Schematic block diagram of the rigid block model for the kinematics of the thrust fault and LKF. In this model the block west of the LKF moved to the north above the thrust, which detaches it from underlying crust. This model is not consistent with several observations. LKF, Landers-Kickapoo fault; SHVF, Southern Homestead Valley fault.

A second difficulty with the rigid block model is the lack of oblique right slip on the thrust fault. The azimuth of the LKF slip vector (N05°E) is not consistent with N38°E directed, pure reverse slip on the thrust fault. In the case of rigid translation between the thrust fault and the LKF (ignoring the SHVF), the average horizontal slip vector (the appendix, part 1) of 144 cm along the LKF would resolve to 78 cm right slip along the thrust (in addition to a dip-slip component), far greater than we observed (Figure 5 and Table 1). Furthermore, when the SHVF slip is taken into consideration, the problem becomes one of three rigid blocks; the block west of the LKF, the block between the LKF and SHVF, and the block east of the SHVF. When a "displacement-space" diagram (similar to the velocity-space diagrams of plate tectonics) is drawn for these three blocks using the maximum dextral offsets along the LKF and SHVF, the resultant slip vector across the thrust fault is over 4 m in magnitude (Figure 10). This slip vector resolves to a horizontal shortening component of 3 m and a dextral component of 3.3 m on the thrust fault, which are much larger than we observed (Figure 5 and Table 1). Furthermore, the ratio of horizontal shortening (or net dip slip) to right slip predicted by this diagram is close to unity and therefore much smaller than we document (Table 1). The lack of right slip on the thrust fault marks a discrepancy in horizontal slip vectors that suggests that the right slip on the LKF/SHVF was not directly transferred onto the thrust fault through rigid block translation.

A third problem with the rigid block interpretation regards the relative vertical offsets along the faults in the JVF-HVF

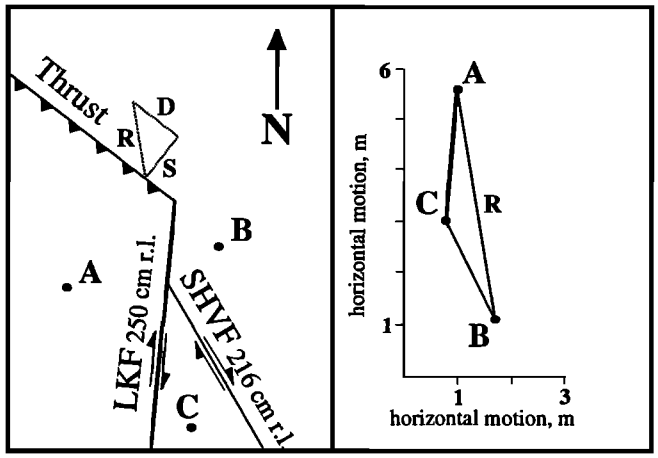

Figure 10. Schematic "displacement-space" vector diagram for the JVF-HVF stepover. On the left, the N05°E LKF, the N27°W SHVF, and the N52°W thrust fault separate three blocks, on which three points (A, B, C) are displaced by the maximum dextral displacements measured on the LKF and SHVF (250 cm and 216 cm, respectively). On the right, the displacement vectors between points A and C (across the LKF) and points C and B (across the SHVF) are added to get the resultant vector of displacement between points A and B across the thrust fault (*R*). This resultant vector is 448 cm directed N10°W, which can be separated into a component of horizontal shortening (*S*) of 300 cm directed N38°E and a dextral component (*D*) of 333 cm on the N52°W thrust fault. LKF, Landers-Kickapoo fault; SHVF, Southern Homestead Valley fault.

stepover. If the entire western side of the LKF had been uplifted on the thrust fault as a rigid block, as the west-side-up motion on the LKF suggests, then the sense of vertical motion along the northern JVF should have been east-side-up, rather than the west-side-up offsets that we document (Figure 2). The west-side-up offset on the northern JVF implies that the thrust fault does not extend southward to the JVF and therefore only underlies a northern fraction of the block west of the LKF. Furthermore, the opposite sense of vertical motion of the northeastern (uplifted on the thrust fault) and southwestern (downdropped on the JVF) edges of the block west of the LKF resembles the vertical component of the elastic displacement field typical of thrust fault ruptures, in which near-field uplift is accompanied by far-field subsidence of the hanging wall block. Although it is beyond the scope of this paper, it may actually be possible to estimate the dimensions, orientation, and slip of the thrust fault at depth from an elastic dislocation model of this deformation pattern.

A fourth problem with the rigid block interpretation concerns the subsurface geometric relations of the LKF and thrust. A rigid block model predicts that the LKF terminates downdip at its intersection with the thrust fault, thereby defining a northeastward tapering wedge of crust (Figure 9). If the thrust fault continues to the southwest with a 20° dip, the downdip width of the LKF should increase from zero on its northern end to only 3.5 km at its intersection with the JVF. Even if the thrust steepens to a 45° dip in the shallow subsurface, the LKF would only be 8 km deep at its intersection with the JVF. The aftershocks around the LKF, however, extend more or less uniformly to a depth of about 14 km (Figure 11) [*Hauksson et al.*, 1993]. This distribution implies that the LKF ruptured to about 14 km depth along most of its length, for if it had ruptured only the upper part of the seismogenic crust, variations in stress with depth would have probably been manifest in the aftershock distribution [*Hauksson et al.*, 1993]. This implies that, in the subsurface, the thrust fault is limited to the northern end of the JVF-HVF stepover or that the thrust fault and LKF do not bound a rigid block.

The short, 3-km length of the thrust fault may be another indication that its downdip width is only a few kilometers. The downdip widths of many historical reverse-fault ruptures are smaller than their rupture lengths. For example, the 1945 Mikawa, Japan, earthquake was caused by a thrust rupture 12 km long and 11 km wide [*Ando*, 1974]. Of 67 historical, nonsubduction zone earthquakes of $M > 4.5$ with a reverse component of motion and known rupture widths, only 12 do not have length greater than width [*Wells and Coppersmith*, 1994]. The aspect ratio (ratio of length to width) of these ruptures averages 1.9 (1.8 for pure reverse ruptures and 2.1 for oblique reverse/strike-slip ruptures). This suggests that the downdip widths of historical reverse-fault ruptures are typically half the rupture length and almost always smaller than the rupture length. The common excess of length relative to width suggests that it is unlikely that the 3-km-long thrust fault extends with a 9-km downdip width from its surficial trace to an intersection with the JVF.

Given these significant problems, it does not seem that the thrust fault and LKF/SHVF intersect and transfer slip in a rigid block fashion. We propose that the secondary thrust rupture is limited in the shallow subsurface to the northern end of the JVF-HVF stepover, and we hypothesize that failure of the thrust was induced by static or dynamic stresses that resulted from dextral shear along the LKF/SHVF and the rapid termination of LKF/SHVF right slip at the southern end of the HV slip gap. This abrupt termination is indicated by the rate of decrease in slip per rupture length (the appendix, part 5), which is, on average, more than 4 times higher along ruptures that terminate at the HV slip gap than along ruptures which terminate elsewhere in the JVF-HVF stepover (Table 2). This value of about 2×10^{-3} m/m for the northern end of the LKF may have concentrated shear stresses that induced failure of the thrust. Furthermore, *Hauksson*'s [1994] analysis of aftershocks showed that the postmainshock maximum principal stresses along the LKF and HVF were N40°E and N46°E, respectively. These are the most easterly trending stress values for the entire Landers rupture zone and are nearly perpendicular to the thrust fault, further supporting the idea that the thrust fault rupture was induced by stresses resulting from dextral shear along the Landers rupture. Static and dynamic models of the ruptures would be necessary to determine whether or not this "induced-slip" model could explain the nearly pure dip slip we observe on the thrust fault, but these are beyond the scope of this paper.

It is worth noting that our interpretation of the relation between the LKF/SHVF and thrust fault is comparable to the interpretation of *Peltzer et al.* [1994] of the JVF-HVF stepover based on synthetic aperture radar interferometry. They suggest the block between the LKF and northern JVF behaved rigidly and was tilted 0.01° to the southwest about a N20°W axis and argue that the vertical displacements on the LKF and thrust fault were responsible for this tilt [*Peltzer et*

al., 1994]. This interpretation implies that the block west of the LKF behaved rigidly, similar to the rigid block model discussed above. However, we propose that the thrust fault was not necessary to produce this tilt, since it can be explained solely by the vertical displacements along the JVF and LKF. If the western side of the JVF and the eastern side of the LKF are held fixed, these vertical offsets yield southwest directed tilts with N20°W axes of from 0.01° to 0.05° (Figure 2). In addition, the interferogram that implies this tilt is only clear in the southwestern part of the block west of the LKF, due to a loss of coherence in the northeastern part near the thrust fault [*Peltzer et al.*, 1994, Figure 5]. This suggests that the rigid tilt was confined to the southern part of the block between the LKF and JVF and is consistent with our interpretation that the thrust fault is limited to the northern end of the JVF-HVF stepover and does not bound a rigid block with the LKF.

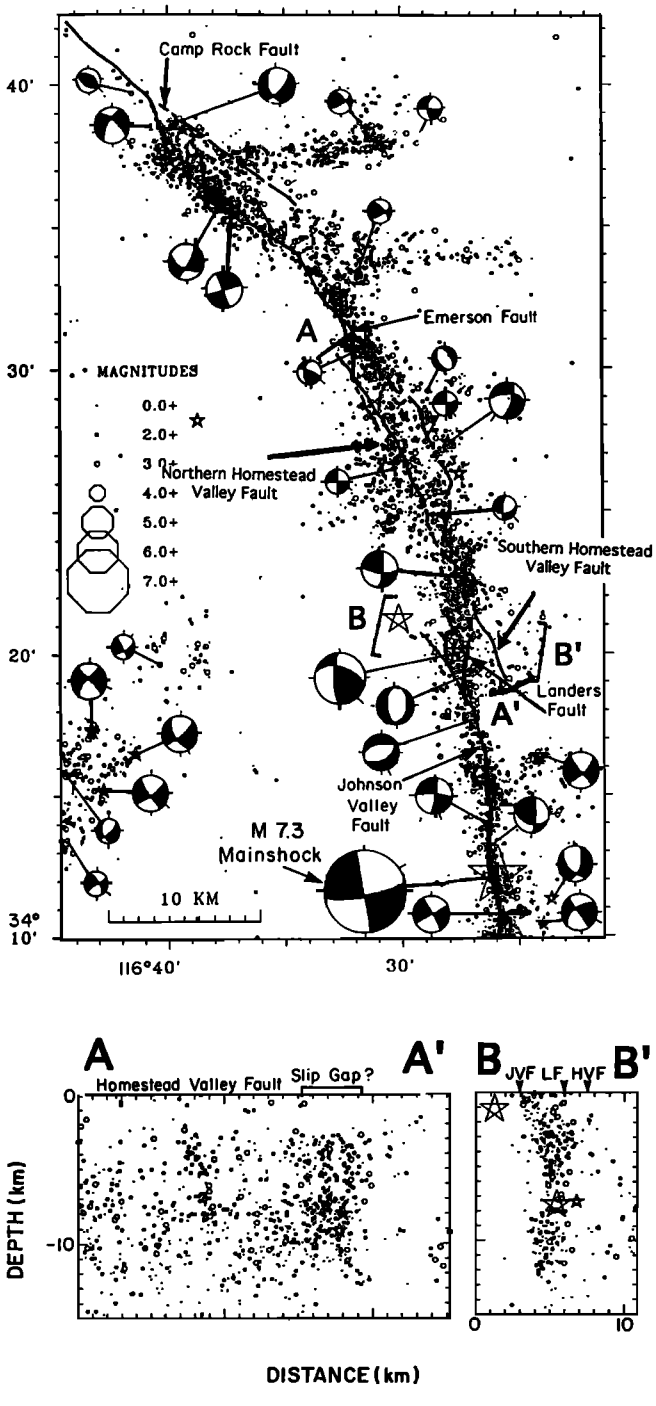

Figure 11. Map and two cross sections through aftershocks of the Landers earthquake (adapted from *Hauksson et al.* [1993]). Focal mechanisms for the larger aftershocks and the mainshock are shown (focal mechanisms for smaller aftershocks are given by *Hauksson* [1994]). Note the dense cluster of aftershocks in the HV slip gap, which extends to 14 km depth.

Table 2. Ratio of Decrease in Slip to Rupture Length Over Which the Decrease Occurs for Each Rupture Termination in the JVF-HVF Stepover

	Ratio
Northern end of JVF	3×10^{-4}
Southern end of SHVF	7×10^{-4}
Southern end of LKF	6×10^{-4}
Average	5.3×10^{-4}
Southern end of NHVF	4×10^{-3}
Northern end of SHVF	1×10^{-3}
Northern end of LKF	2×10^{-3}
Average	2.3×10^{-3}

See the appendix, part 5. Note that ratios are significantly greater for ruptures that terminate at the HV slip gap than for those which terminate elsewhere.

Kinematic Interpretation of the Zone of en Echelon Extension

Several observations support the hypothesis that the en echelon zone of normal faults and tensile fractures that traverses the hill in the HV slip gap is related to the southern termination of the NHVF. First, the northern end of the en echelon zone is within a few hundred meters of the southern surficial termination of the NHVF. Second, the trend of the zone is parallel to the NHVF (Figure 5). Third, the average north-northeast trend of the individual fractures of the zone is oblique to the trend of the NHVF by about 35° to 50°. This, along with the weak left-stepping pattern of the fractures, is consistent with dextral shear along the azimuth of the NHVF. Finally, the slip on the fractures of the en echelon zone generally diminishes southwestward, away from the NHVF. We propose that the en echelon extensional fractures mark a zone of diffuse dextral shear that corresponds to southward propagation of the surficial NHVF rupture. The abrupt termination of the NHVF at the surface, indicated by the rate of decrease in dextral slip per rupture length of about 4×10^{-3} m/m (Table 2 and the appendix, part 5), may have resulted in enough stress to cause the secondary rupture of this zone of en echelon fractures. The lack of strike-slip offset on these fractures, their spatial arrangement, and the minimal extension they accommodate, however, suggest they do not make up a pervasive strike-slip shear zone like those elsewhere along the Landers rupture. As with the thrust fault, static and dynamic models of the ruptures would be necessary to test this "induced-slip" model.

Model of the JVF-HVF Stepover Rupture Pattern

Our kinematic interpretations of the ruptures in the HV slip gap imply that dextral shear in the shallow crust resulted in secondary, non–strike-slip deformation, instead of a

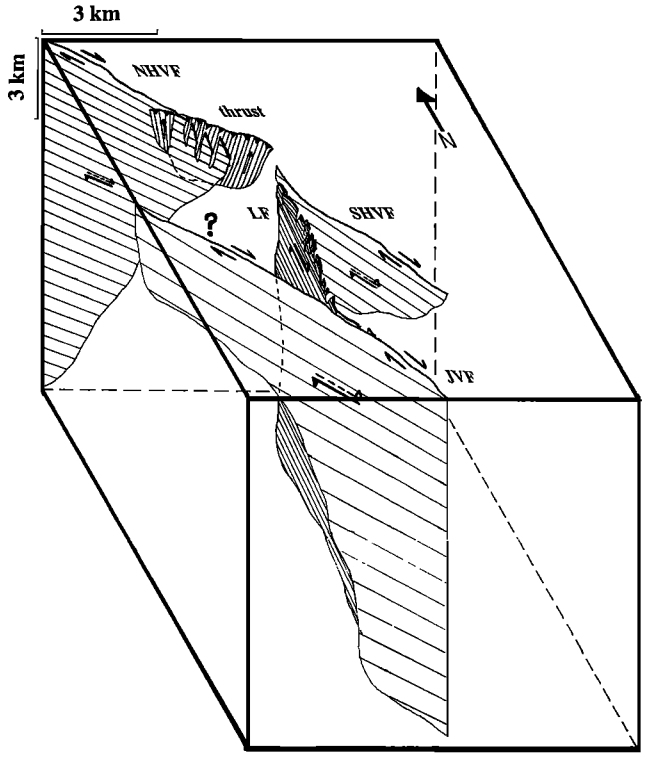

Figure 12. Schematic block diagram of our favored model for fault interaction in the JVF-HVF stepover. The lined planes represent our interpretations of the three-dimensional 1992 rupture surfaces. The thrust fault rupture is limited to the shallow crust and was induced by stress from a right-lateral couple that resulted, in part, by the slip on the LKF, although these two faults do not intersect or bound a rigid block. The NHVF propagated southward into the slip gap as the en echelon zone of extension, which appears to have been induced by a right-lateral couple as well. The question mark represents the uncertainty regarding the geometry of ruptures below the near surface, although we tentatively show an absence of a throughgoing rupture that is similar to the discontinuity we interpret at the surface. NHVF, Northern Homestead Valley fault; LF, Landers-Kickapoo fault; SHVF, Southern Homestead Valley fault; JVF, Johnson Valley fault.

through-going right-lateral rupture. The stresses created by right slip along the LKF/SHVF and by the NHVF and the rapid termination of this right slip (Table 2) may have induced the failure of the thrust fault and the zone of en echelon extension but did not produce a continuous connection between the northern and southern strike-slip faults or transfer slip via the rigid translation of blocks. This discontinuity in the 1992 dextral rupture indicates that there must have been a barrier to the dynamic rupture propagation.

The three-dimensional rupture pattern implied by our proposed lack of a continuous rupture through the slip gap is shown schematically in Figure 12. In this speculative model, we consider the thrust fault to be limited to the shallow crust and do not connect it with either the LKF or the SHVF. We represent the zone of en echelon extension as a continuation of the NHVF and show it to be contiguous with the NHVF at depth. Our observations do not require this, however, and this zone could be physically separated from the major fault that induced its movement. We also postulate that the northern JVF and SHVF ruptures were limited to the shallow crust, because of the near absence of aftershocks along them (Figures 11 and 12). We do not know the rupture pattern below the thrust fault and zone of en echelon extension in the slip gap (Figure 12). It is simplest to assume that the lack of a throughgoing dextral rupture at the surface reflects a similar discontinuity at depth (as shown in Figure 12), but our geological observations do not preclude other possibilities. There are, however, other sources of evidence that suggest the rupture may have been discontinuous at depth in the slip gap.

There is a cluster of aftershocks in the HV slip gap that is more dense than elsewhere along the Landers rupture zone (Figure 11 and *Hauksson et al.* [1993]), which may indicate that postmainshock stresses in the slip gap were higher than elsewhere. This aftershock cluster could have resulted from a lack of continuous rupture at depth bounded by high-slip ruptures. The terminations of these ruptures could have induced high stresses, an idea that is consistent with the hypothesis of *Mendoza and Hartzell* [1988] that aftershocks commonly occur in the volume of crust that surrounds the ends of high-slip ruptures. A similarly dense aftershock cluster occurred between the southern end of the JVF and the northern end of the Eureka Peak fault, where no throughgoing rupture occurred [*Sieh et al.*, 1993; *Hauksson et al.*, 1993]. The dense cluster of aftershocks, however, does not require a gap in continuous faulting. It could also have resulted from stresses produced by a slip deficit along a continuous dextral rupture or by a stress heterogeneity due to the bend in strike from the LKF/SHVF to the NHVF along a continuous rupture.

Another source of evidence that suggests there may not have been a throughgoing rupture in the HV slip gap is the lack of a seismic waveguide there after the earthquake. North and south of the slip gap there are narrow, low-velocity zones along the Landers ruptures that trap short-wavelength shear waves of aftershocks that occur along the fault zone [*Li et al.*, 1994]. *Li et al.* [1994] interpret these to reflect the existence of a continuous, low-velocity plane at depth but are not certain whether this plane is the 1992 rupture zone or a pre-1992 "geological wear zone." In the area of the fault bend from the LKF to the HVF, there is no waveguide from the surface to a depth of 6 km [*Li et al.*, 1994]. Although this may correlate with the surficial rupture discontinuity in the slip gap, this absence of a waveguide continues north of the slip gap along the entire NHVF, in contrast to the surficial rupture. We therefore hesitate to use this intriguing approach to identify the pattern of rupture at depth but recognize the possibility that the lack of a waveguide in the slip gap could indicate a fault discontinuity.

Thus the aftershocks and the lack of a seismic waveguide in the HV slip gap are consistent with a discontinuous rupture at depth but do not require one. The rupture discontinuity, which we propose exists in the near surface of the slip gap, may therefore continue at depth.

Geophysical Evidence of the Slip Distribution in the HV Slip Gap

The deficiency in both right slip and net slip on the surficial ruptures of the HV slip gap relative to the dextral ruptures to the north and south may reflect a similar deficit in slip at depth. Although our observations do not constrain the rupture pattern at depth, models of seismic and geodetic data

offer insight into the amount of slip that occurred beneath the surficial slip gap.

Some analyses of seismic [*Kanamori et al.*, 1992; *Sieh et al.*, 1993; *Campillo and Archuleta*, 1993; *Dreger*, 1994] and geodetic [*Hudnut et al.*, 1994] data resolve a deficit in the average slip at depth on the ruptures of the slip gap, which suggest that the surficial deficit continues to the base of the seismogenic crust. However, other analyses of seismic [*Velasco et al.*, 1994], geodetic [*Freymueller et al.*, 1994], and synthetic aperture radar interferometry [*Massonnet et al.*, 1993] data vaguely show two high-slip sections of rupture north and south of the slip gap but do not indicate that the slip throughout the slip gap is below 2 m. The detailed inversions of geophysical data by *Cohee and Beroza* [1994] and *Wald and Heaton* [1994] also suggest that the slip gap was a patch of lesser right slip between two high-slip sections of rupture but indicate that 3 m of slip occurred in the shallow crust of the slip gap, which is much more than we document.

All of these geophysical models of the displacement in the slip gap are nonunique due to the assumptions they incorporate and have limited spatial and temporal resolution due to the smoothing of data they employ. These models are therefore ambiguous and inconsistent. Although some show a slip deficit at depth that is consistent with the discontinuity in rupture that we propose, others suggest that the rupture was throughgoing. Therefore we cannot conclude whether the surficial slip deficit or rupture discontinuity continues at depth on the basis of geophysical models.

Sequence of Events During the 1992 Landers Earthquake

The sequence of ruptures propagating into and through the HV slip gap can be inferred from the geometric relations of the faults. The orientation and transport direction of the thrust fault suggest that it ruptured in response to dextral slip on the LKF, which requires that rupture of the LKF preceded the rupture of the thrust fault. The NHVF seems to have ruptured after the thrust fault, because the thrust fault continues without diminution of offset for 500 m northwestward of its intersection with the NHVF (Figure 5). If the NHVF ruptured first, the abrupt southern termination of its rupture would have produced substantial extension along the westernmost segment of the thrust fault that would have inhibited a contractional rupture. The zone of en echelon extension also seems to have ruptured after the thrust fault, because at least one fracture within it cut the thrust scarp without being offset (location p; Figure 5). The zone of extension may have also ruptured after the NHVF, because it seems to have been a secondary continuation of the NHVF south of its abrupt termination.

This geologically determined sequence implies a general northward propagation of rupture, and is therefore consistent with the unilateral northward propagation determined seismologically [e.g., *Kanamori et al.*, 1992]. The rupture of the zone of en echelon extension after the NHVF is an exception to this general northward propagation. However, this fine detail of the rupture dynamics, which can be inferred from geological data, probably cannot be resolved from the geophysical data.

Other aspects of the rupture propagation in the detailed model of *Wald and Heaton* [1994] can be compared with our interpretations. In Figure 13 we reproduce their spatiotemporal development of the Landers rupture [*Wald and Heaton*, 1994, Figure 16], which shows the time progression of the Landers rupture for their combined dislocation model. In this figure the rupture propagates from the hypocenter to the slip gap in 6 s but lingers for 4 s, while 4 m of slip occur on the faults within the JVF-HVF stepover. In the 10–11 s interval after the initiation of rupture, a 1-m burst of slip occurs in the upper 5 km of the HV slip gap. We suggest that this burst reflects the rupture of the thrust fault. Simultaneously, 0.5 m of isolated slip occurs at a depth of 10–15 km in the slip gap. We suggest that this reflects initiation of rupture on the NHVF that may have been discontinuous with the ruptures south of the slip gap. The continuation of shallow slip in the slip gap during the next 2 s and its connection with the slip to the north on the NHVF are consistent with the southeastward rupture of the en echelon fractures after the initial rupture of the NHVF.

Although the correlations of our interpretations with the model of *Wald and Heaton* [1994] are highly speculative and can be no more accurate than the models themselves, the correlation of geologic and seismologic models is intriguing. If the details of the rupture propagation inferred in their model do, in fact, relate to localized characteristics of the rupture that we have documented at the surface, then a major gap between geological and geophysical interpretations of coseismic processes may have been bridged for the first time.

Tectonic Development of the Slip Gap

Although our study did not focus on the geologic evidence of previous faulting in the JVF-HVF stepover, we made several observations that have implications for its long-term tectonic development. Based on these observations, we propose that the LKF and the secondary faults in the HV slip gap are less mature than the JVF and NHVF/SHVF and that they are in the process of connecting the JVF and HVF strike-slip systems.

The NHVF has a total dextral offset of about 300 m, based on an offset lens of marble [*Dibblee*, 1967], offset drainages and shutter ridges, and bedrock and geomorphic offsets of a small hill [*Zachariasen and Sieh*, 1994]. The SHVF may have a similar amount of previous right slip, given its similar topographic expression and an offset shutter ridge on the southeast side of the hill in the slip gap (Figures 2 and 5). These 300 m of cumulative slip would have been produced in about 100 1992-sized ruptures and appears adequate to form integrated, continuous fault zones. The JVF also has a throughgoing trace and displays truncations and offsets of geologic units along it [*Dibblee*, 1967], which suggests that it has also had substantial previous right slip. Both the JVF and the HVF strike-slip systems have been active in the Holocene [*Hecker et al.*, 1993; *Lindvall and Rockwell*, 1993; *Herzberg and Rockwell*, 1993].

The LKF and smaller faults in the HV slip gap seem to have much less cumulative offset than the JVF and HVF systems. Although the LKF is a preexisting structure [*Sowers et al.*, 1994; *Lindvall and Rockwell*, 1993], both its lack of conspicuous tectonic landforms and the complex en echelon character of its trace (Figure 2) suggest that it has significantly less cumulative offset than the more integrated traces of the NHVF, SHVF, and JVF. This interpretation is supported by the correlation between smoothness of fault traces and cumulative offset [*Wesnousky*, 1988; *Tchalenko*, 1970]. The lack of deflection of the JVF trace at its conflu-

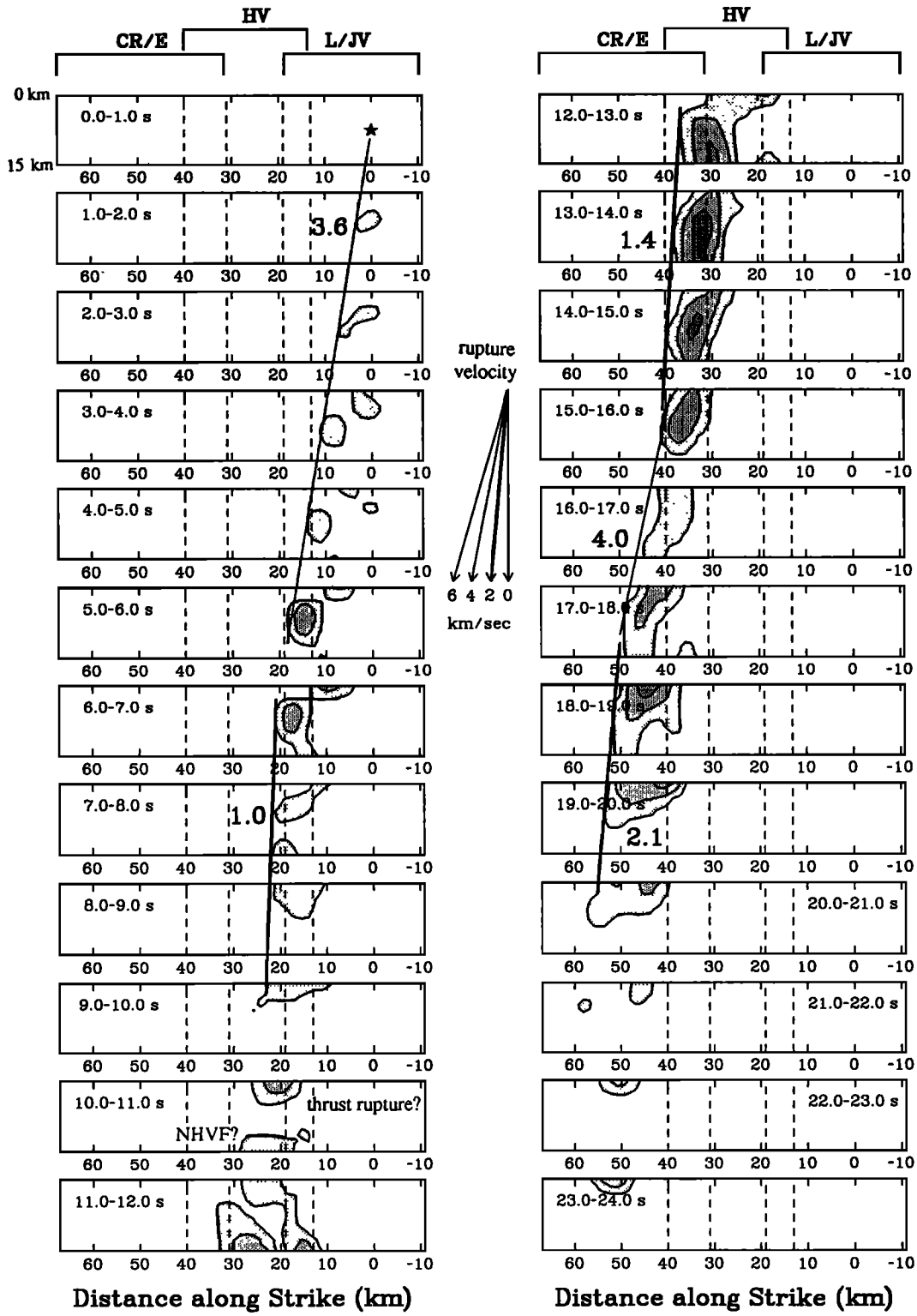

Figure 13. Spacio-temporal progression of the Landers rupture for a combined dislocation model from *Wald and Heaton* [1994] (adapted from their Figure 16). Each rectangle is the cross section of the rupture plane and shows dextral slip for a different 1-s interval. The model incorporates strong ground motion, teleseismic body waves, and geodetic data. We propose that the shallow burst of slip in the slip gap 10–11 s into the earthquake is the thrust fault rupture and that the deep slip during this same interval is the initiation of rupture on the NHVF. Depth is from 0 to 15 km, and rupture is divided into three segments; CR/E (Camp Rock/Emerson faults), HV (Homestead Valley fault), and L/JV (Landers-Kickapoo/Johnson Valley faults). Contour interval is 0.5 m of slip. Lines traversing several rectangles indicate periods of nearly constant rupture velocity.

ence with the LKF also argues that the total offset on the LKF is small. Furthermore, there is no gravity anomaly associated with the LKF, whereas the JVF has a gravity anomaly that suggests it is associated with a bedrock scarp buried by alluvium [*Sowers et al.*, 1994]. If both faults typically rupture with similar-sized vertical offsets as they did in 1992, the lack of a geophysically apparent bedrock scarp along the LKF suggests that it has ruptured fewer times than the JVF.

The thrust fault may have ruptured in as few events as the LKF, if it is mechanically related to the LKF. Although we observed old scarps along the trace of the thrust fault, these were only several times the size of the 1992 scarps. The 200-m-high hill in the hanging wall of the thrust fault, however, would imply much more uplift. More than 500 thrust ruptures of average 1992 vertical offset are required to have fully uplifted this hill, which is more rupture events than the LKF or even the JVF, SHVF, or NHVF have probably sustained. However, there is no evidence that precludes uplift of this hill by mechanisms other than the thrust fault, and there is evidence that the hill may have existed before the thrust fault was active. The 300-m bedrock and geomorphic offsets of a smaller hill across the NHVF show that the HVF strike-slip system was active after creation of the present topography of the region [*Zachariasen and Sieh*, 1994]. The hill in the slip gap could have also existed before the HVF system was active and would have therefore existed before the JVF-HVF stepover, LKF, and thrust fault were active (assuming they are all mechanically related). We therefore consider it possible that the thrust fault has ruptured as few times as the LKF and the hill in the slip gap may not have been uplifted entirely in concert with slip on the thrust fault.

The fractures in the en echelon zone of extension in the slip gap also appear to have little cumulative slip. We compared the size and sense of the 1992 vertical offsets with the steepness and sense of topographic relief around each fracture and found that virtually none of the fractures could have sustained more than 10 previous 1992-sized ruptures. Although these estimates do not take into account heavy erosion, they do suggest that the normal fractures have ruptured far fewer times than the JVF or NHVF/SHVF. This, along with the kinematic relationship between the extension and the NHVF in 1992, implies that the zone of extension is an immature southern continuation of the NHVF. The individual extensional fractures may be similar to splays of a strike-slip fault that have not yet integrated into a continuous fault zone due to a lack of sufficient cumulative slip. Similar discontinuous en echelon surficial shears are produced by strike slip on a subsurface fault in shear box and Reidel experiments with granular material, which eventually integrate into an irregular but continuous fault zone as cumulative displacement increases [*Tchalenko*, 1970]. Fault zones in the Earth's crust are thought to evolve from initial en echelon geometries in a similar fashion [*Wesnousky*, 1988; *Bjarnasson et al.*, 1993].

Thus it seems that the JVF and the HVF systems have more cumulative offset than the LKF, the en echelon zone of extension, and possibly the thrust fault. This precludes the possibility that rupture of the LKF-thrust-en echelon system could have been a characteristic feature of all the previous ruptures of the JVF and HVF. Therefore we propose that the connection between the JVF and HVF strike-slip systems is in the process of developing. The 1992 rupture pattern suggests this even more strongly, because no throughgoing dextral rupture broke through the slip gap and the only right slip between the LKF/SHVF and NHVF was accommodated by secondary faulting. This inability to break through in 1992 indicates that the connection between the JVF and HVF is not yet fully functional. If the JVF-HVF stepover was complete, the LKF would have transferred its several meters of right slip to the NHVF via a continuous rupture, rather than terminating and resulting in non–strike-slip deformation, and would exhibit more maturity. There was probably a physical barrier that prevented the LKF from transferring slip with a throughgoing rupture, such as the 30° bend in strike between it and the NHVF or perhaps an absence of a continuous, preexisting fault zone. Such a barrier would be both the result and indication of the immaturity and incompleteness of the connection between the JVF-HVF stepover.

The juvenile LKF-thrust-en echelon system therefore seems to represent a nascent connection, which in 1992 and in a limited number of previous ruptures has begun to connect the JVF and HVF systems. The 1992 rupture pattern may therefore mark the early stages of the transition to a single, contiguous strike-slip system. This interpretation is consistent with the observation of *Nur et al.* [1993] that recent earthquake ruptures in the Eastern California shear zone have been on northerly trending faults that have less cumulative slip than the northwest trending faults in the zone.

Summary and Conclusions

We document a gap in dextral surficial rupture along a 3-km-long segment of the Landers earthquake rupture. Along this gap, is a northwest trending, southwest dipping thrust fault rupture, which has an average of less than 1 m net dip slip and virtually no oblique right slip. Our observations suggest that this thrust fault does not bound a rigid block that moved to the north along the Landers-Kickapoo fault but seems to be a secondary effect of dextral shear that is confined to the shallow crust of the northern end of the Johnson Valley fault–Homestead Valley fault stepover. A zone of en echelon extensional ruptures also accommodates less than 0.5 m of N81°W extension in the gap, which seems to have been produced as a secondary effect of dextral shear that can be considered an immature southward continuation of the Northern Homestead Valley fault. These induced-slip interpretations of the rupture kinematics could be tested by elastic dislocation models, which are beyond the scope of this paper. The combined right slip of less than 1 m accommodated by these secondary ruptures and their combined net slip are significantly smaller than the right slip on the dextral ruptures to the north and south, which implies that there is a deficit in surficial slip along this segment of the Landers rupture.

The lack of throughgoing dextral rupture that seems to have resulted in the secondary thrust and extensional ruptures suggests that there was a discontinuity in the Landers rupture at the north end of the Johnson Valley fault–Homestead Valley fault stepover. This discontinuity implies that the dynamic propagating rupture was prevented from breaking through the crust, and we propose that this is because the connection between the Johnson Valley and

Homestead Valley strike-slip systems is incomplete. This hypothesis is supported by the apparent immaturity of the faults that compose the connection between the strike-slip systems. Despite this absence of a complete connection, the Landers rupture managed to continue along the Northern Homestead Valley fault and other major faults north of the slip gap. This suggests that coseismic ruptures can jump across fault segments that are not fully connected and therefore that fault segment length is not, by itself, a reliable indicator of future rupture dimensions.

Our observations do not resolve whether an absence in continuous dextral rupture or a deficit in net slip occurred at greater depth along this segment of the rupture. Aftershocks and the lack of a seismic waveguide along this segment suggest that there could have been a gap in continuous faulting, but this is not conclusive. Geophysical analyses of seismic and geodetic data show this segment as both a lack of right slip that extends throughout the seismogenic crust and a patch of lessor slip between two high-slip sections of a continuous dextral rupture. The ambiguities of these analyses prevent us from using them to determine whether there is a slip deficit or rupture discontinuity throughout the seismogenic crust in the slip gap. Our interpretation of the sequence of ruptures in the surficial gap, however, seems to correlate with the geophysical models of the dynamic rupture propagation.

Appendix

1. The average displacement for a fault rupture segment is calculated as follows: the rupture is divided into segments defined by the locations of offset measurements (there is one segment for each measurement and the ends of each segment are defined by the midpoints between locations of measurements), each offset is then multiplied by its segment length, these products are then added together for the entire fault, and finally the sum is divided by the total fault length to get the length-weighted average fault displacement.

2. The average trend of the extensional fractures is calculated as follows: for a length-weighted average, the trend of each fracture is multiplied by its length and the values are summed and divided by the total length (result is N09°E). An offset-weighted average can also be calculated as follows: the trend of each fracture is multiplied by its vertical offset and the values are summed and divided by the total vertical offset (result is N10°E). The similarity of these two averages shows that extensional fractures are dominantly north-northeast trending.

3. To estimate the maximum N81°W horizontal extension across the en echelon normal faults, we summed the extension on fracture splays that are arranged in a parallel series. We added the extension on fractures that could be intersected by semistraight lines across the hill along the average extension direction and found that the greatest extension was always much less than 0.5 m. Admittedly, this estimate of the extension has limited accuracy given the assumed 75° dip, the exclusion of open fissure widths, the use of maximum vertical offsets instead of average offsets, and the difficulty of arranging the fractures into a parallel series. However, our goal was to define an upper limit for the amount of extension and we feel that the 0.5 m maximum limit is accurate for this purpose.

4. The correlation coefficient for the trends of the tensile fractures is calculated as follows: the ratio of the number of fractures with trends of a certain range to the total number of fractures is divided by the ratio of that given range in trend to the overall range in trend (180°).

5. The ratio of the decrease in slip to the rupture length over which the decrease occurs is calculated as follows: for the end of a given rupture, all of the dextral slip values that are decreasing in the direction of the rupture termination (usually within several km of the termination) are divided individually by the distance of the measurement site from the end of the rupture, and these values are then averaged for each fracture terminus (Table 2). These values can be considered to be twice the longitudinal strain exerted on either side of the fault by the termination of the rupture.

Acknowledgments. We thank Anne Lilje for major help on figures and data tabulation, Egill Hauksson for Figure 11, and Dave Wald and Tom Heaton for Figure 13. We also thank Gilles Peltzer, Dave Wald, Egill Hauksson, Mark Abolins, Rob Brady, and Judy Zachariasen for helpful discussions and Anthony Crone, Wayne Thatcher, and an anonymous reviewer for helpful reviews. This study was funded by the Jet Propulsion Laboratory-Director's Discretionary Fund 7300064703235 and the Southern California Earthquake Center/National Science Foundation grant EAR-8920136. Contribution 5439, Division of Geological and Planetary Sciences, California Institute of Technology.

References

Ando, M., Faulting in the Mikawa earthquake of 1945, *Tectonophysics*, *22*, 173–186, 1974.

Bjarnasson, I. T., P. Cowie, M. Anders, L. Seeber, and C. Scholz, The 1912 Iceland earthquake rupture: Growth and development of a nascent transform system, *Bull. Seismol. Soc. Am.*, *83*, 416–435, 1993.

Bryant, W. A., Fault evaluation report FER-234: Surface fault rupture along the Johnson Valley, Homestead Valley, and related faults associated with the *Ms* = 7.5 28 June 1992 Landers earthquake, *Spec. Publ. Calif. Div. Mines Geol.*, *42*, 1992.

Campillo, M., and R. J. Archuleta, A rupture model for the 28 June 1992 Landers, California, earthquake, *Geophys. Res. Lett.*, *20*, 647–650, 1993.

Cohee, B. P., and G. C. Beroza, Slip distribution of the 1992 Landers earthquake and its implications for earthquake source mechanics, *Bull. Seismol. Soc. Am.*, *84*, 692–712, 1994.

Dibblee, T. W., Geologic map of the Emerson Lake Quadrangle, San Bernardino County, California, *U.S. Geol. Surv. Misc. Geol. Invest. Map*, *I-490*, 1967.

Dreger, D. S., Investigation of the rupture process of the 28 June 1992 Landers earthquake utilizing TERRAscope, *Bull. Seismol. Soc. Am.*, *84*, 713–724, 1994.

Freymueller, J., N. E. King, and P. Segall, The coseismic slip distribution of the Landers earthquake, *Bull. Seismol. Soc. Am.*, *84*, 646–659, 1994.

Hart, E. W., W. A. Bryant, and J. A. Treiman, Surface faulting associated with the June 1992 Landers earthquake, California, *Calif. Geol.*, *46*, 10–16, 1993.

Hauksson, E., State of stress from focal mechanisms before and after the 1992 Landers earthquake sequence, *Bull. Seismol. Soc. Am.*, *84*, 917–934, 1994.

Hauksson, E., L. M. Jones, K. Hutton, and D. Eberhart-Phillips, The 1992 Landers earthquake sequence: seismological observations, *J. Geophys. Res.*, *98*, 19,835–19,858, 1993.

Hecker, S., T. E. Fumal, T. J. Powers, J. C. Hamilton, C. D. Garvin, D. P. Schwartz, and F. R. Cinti, Late Pleistocene-Holocene behavior of the Homestead Valley fault segment—1992 Landers, CA surface rupture, *Eos Trans. AGU*, *74*(43), Fall Meeting suppl., 612, 1993.

Herzberg, M. and T. Rockwell, Timing of past earthquakes on the northern Johnson Valley fault and their relationship to the 1992 rupture, *Eos Trans. AGU*, *74*(43), Fall Meeting suppl., 612, 1993.

Hudnut, K. W., et al., Coseismic displacements of the 1992 Landers earthquake sequence, *Bull. Seismol. Soc. Am.*, *84*, 625–645, 1994.

Johnson, A. M., R. W. Fleming, and K. M. Cruikshank, Shear zones formed along long, straight traces of fault zones during the 28 June 1992 Landers, California, earthquake, *Bull. Seismol. Soc. Am.*, *84*, 499–510, 1994.

Kanamori, H., H.-K. Thio, D. Dreger, E. Hauksson, and T. Heaton, Initial investigations of the Landers, California, earthquake of 28 June 1992 using TERRAscope, *Geophys. Res. Lett.*, *19*, 2267–2270, 1992.

Li, Y.-G., J. E. Vidale, K. Aki, C. J. Marone, and W. H. K. Lee, Fine structure of the Landers fault zone: segmentation and the rupture process, *Science*, *265*, 367–370, 1994.

Lindvall, S., and T. K. Rockwell, Recurrent Holocene faulting along the Johnson Valley portion of the 1992 Landers earthquake surface rupture, *Geol. Soc. Am. Abstr. Programs*, *25*, 70, 1993.

Massonnet, D., M. Rossi, C. Carmona, F. Adragna, G. Peltzer, K. Feigl, and T. Rabaute, The displacement of the Landers earthquake mapped by radar interferometry, *Nature*, *364*, 138–142, 1993.

Mendoza, C., and S. H. Hartzell, Aftershock patterns and main shock faulting, *Bull. Seismol. Soc. Am.*, *78*, 1438–1449, 1988.

Nur, A., R. Hagai, and G. C. Beroza, The nature of the Landers-Mojave earthquake line, *Science*, *261*, 201–203, 1993.

Peltzer, G., K. W. Hudnut, and K. L. Feigl, Analysis of coseismic surface displacement gradient using radar interferometry: New insights into the Landers earthquake, *J. Geophys. Res.*, *99*, 21,971–21,981, 1994.

Sieh, K., et al., Near-field investigations of the Landers earthquake sequence, April to July 1992, *Science*, *260*, 171–176, 1993.

Sowers, J. M., J. R. Unruh, W. R. Lettis, and T. D. Rubin, Relationship of the Kickapoo fault to the Johnson Valley and Homestead Valley faults, San Bernardino County, California, *Bull. Seismol. Soc. Am.*, *84*, 528–536, 1994.

Tchalenko, J., Similarities between shear zones of different magnitudes, *Geol. Soc. Am. Bull.*, *81*, 1625–1640, 1970.

Velasco, A. A., C. J. Ammon, and T. Lay, Empirical Green function deconvolution of broadband surface waves: Rupture directivity of the 1992 Landers, California (M_W = 7.3), earthquake, *Bull. Seismol. Soc. Am.*, *84*, 735–750, 1994.

Wald, D. J., and T. H. Heaton, Spatial and temporal distribution of slip for the 1992 Landers, California earthquake, *Bull. Seismol. Soc. Am.*, *84*, 668–691, 1994.

Wells, D. L., and K. J. Coppersmith, New empirical relationships among magnitude, rupture length, rupture width, rupture area, and surface displacement, *Bull. Seismol. Soc. Am.*, *84*, 974–1002, 1994.

Wesnousky, S., Seismological and structural evolution of strike-slip faults, *Nature*, *335*, 340–343, 1988.

Zachariasen, J., and K. Sieh, The kinematics of slip transfer between two en echelon strike-slip faults: A case study from the 1992 Landers earthquake, southern California, *J. Geophys. Res.*, in press, 1995.

K. Sieh and J. A. Spotila, 170-25, Division of Geological and Planetary Sciences, California Institute of Technology, Pasadena, CA 91125. (e-mail: sieh@seismo.gps.caltech.edu; spot@legs.gps.caltech.edu)

(Received March 11, 1994; revised August 18, 1994;
accepted September 14, 1994.)